Research Article

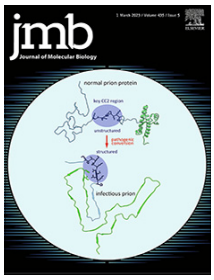

Selenoprotein S Interacts with the Replication and Transcription Complex of SARS-CoV-2 by Binding nsp7

Farid Ghelichkhani, Fabio A. Gonzalez, Mariia A. Kapitonova and Sharon Rozovsky *

Department of Chemistry and Biochemistry, *University of Delaware, Newark, DE 19716, USA*

Correspondence to Sharon Rozovsky: *rozovsky@udel.edu (S. Rozovsky) @sharonrozovsky (S. Rozovsky)*
https://doi.org/10.1016/j.jmb.2023.168008
Edited by M.F. Summers

Abstract

The severe acute respiratory syndrome coronavirus-2 (SARS-CoV-2) replicates and evades detection using ER membranes and their associated protein machinery. Among these hijacked human proteins is selenoprotein S (selenos). This selenoprotein takes part in the protein quality control, signaling, and the regulation of cytokine secretion. While the role of selenos in the viral life cycle is not yet known, it has been reported to interact with SARS-CoV-2 nonstructural protein 7 (nsp7), a viral protein essential for the replication of the virus. We set to study whether selenos and nsp7 interact directly and if they can still bind when nsp7 is bound to the replication and transcription complex of the virus. Using biochemical assays, we show that selenos binds directly to nsp7. In addition, we found that selenos can bind to nsp7 when it is in a complex with the coronavirus's minimal replication and transcription complex, comprised of nsp7, nsp8, and the RNA-dependent RNA polymerase nsp12. In addition, through crosslinking experiments, we mapped the interaction sites of selenos and nsp7 in the replication complex and showed that the hydrophobic segment of selenos is essential for binding to nsp7. This arrangement leaves an extended helix and the intrinsically disordered segment of selenos—including the reactive selenocysteine—exposed and free to potentially recruit additional proteins to the replication and transcription complex.

Introduction

The serum level of selenium, which is a trace element and micronutrient essential for human health, strongly correlates with COVID-19 recovery.[1–2] In humans, selenium is primarily utilized in selenoproteins, which are often associated with cellular stress management.[3] Selenoproteins are critical in other aspects of human health, such as inflammatory response, immune health, cancer, and aging.[4–5] These proteins are also known to take part in viral invasions. Several of them interact with SARS-CoV-2 viral proteins or are modified or suppressed by viral processes.[6] These selenoproteins include glutathione peroxidase 1 and 4, which protect cells from reactive oxygen species (ROS)[7]; selenoprotein I, which is involved in lipid synthesis,[8] selenoprotein F, which assists in protein folding[9]; selenoprotein K, which acts in protein quality control, protein palmitoylation and immune response,[10] and selenoprotein S (selenos, VIMP, SEPS1), which functions in protein quality control[11–12] and signaling.[13] A detailed look at its various cellular functions and associations can be found in a recent review.[14]

Selenos is also a member of the NF-kappaB, NFAT, and MAPK signaling pathways[13] and is known to suppress cytokine and growth factor secretion.[15–16] In addition, genetic polymorphism is tightly linked to vascular and cardiovascular

health,[17–18] cancer,[19–21] diabetes[22–27] and metabolic disorders.[28] Selenos was found in multiple independent studies to be tied to diverse viral infections, such as enterovirus 71,[29] cytomegalovirus,[30] and SARS-CoV-2.[31] It is located in the ER membrane[32] and is a member of the endoplasmic reticulum-associated protein degradation (ERAD) pathway that coronaviruses hijack because it is critical for their replication.[33] Therefore, selenos has been assumed to play a role in the virus's ability to evade degradation of its proteins. In addition, selenos's ERAD protein partner, VCP/p97 ATPase, is essential for coronavirus's exit from endosomes.[34–35] However, the SARS-CoV-2 interactome maps with human proteins revealed that, in contrast to the simplistic view that selenos acts by modulating p97, selenos itself is actually an interaction partner of several viral proteins (Supporting Information Table S1). Multiple reports of the interactions of individually expressed SARS-CoV-1 and SARS-CoV-2 proteins with human host proteins documented selenos interactions with coronavirus's proteins: most frequently nsp7, orf7a, and orf7b, but occasionally also nsp4, nsp6, and nsp3.[36–42] Nsp7 is part of the viral replication and transcription complex (RTC) but also acts as a transcription factor.[43] Orf7a and orf7b disrupt STAT1 and STAT2 signaling pathways, hindering interferon signaling.[44] Nsp3, nsp4, and nsp6 drive the formation of membranous structures essential for coronaviruses replication,[41,45] in which the RTC hides from the immune system. These viral proteins are also part of the central pore through which newly synthesized RNA is exported from these membranous structures.[46]

These studies profiled protein partners of individual proteins by expressing them one at a time in model cells. However, there is evidence that selenos is also in direct contact with the RTC in infected cells that express the full viral genome.[36] This was shown by proximity labeling without disrupting intracellular membranes or protein complexes for the coronavirus murine hepatitis virus (MHV). The preponderance of evidence suggests that selenos is linked to cellular pathways hijacked by the coronavirus and is points to a likely role of the protein in the virus's life cycle. Yet, the impact of selenos on the virus's replication[47] is unclear as assays of viral replication with selenos siRNA and CRISPR knockout were carried in media formulations that were not supplemnted with selenium, rendering comparisons with unhindered cells unreliable for selenoproteins.[37]

Although selenos was indicated as a protein partner of several SARS-CoV-2 proteins, its precise role or mode of interactions with these viral proteins remain unknown. This is in no small part because selenos has multiple cellular roles, many of which are not well-understood.[14–16] Because all well characterized selenoproteins utilize their selenocysteine (Sec, U) to catalyze chemical reactions, selenos is in all likelihood also an enzyme. We have shown that it is a powerful reductase *in vitro*,[48–49] but the precise cellular role of its Sec *in vivo* remains enigmatic. Narrowing down the cellular role(s) of selenos in COVID-19 is also complicated by the large number of proteins (over 200) found to interact with selenos.[50] Many of these putative protein partners are likely members of large protein complexes and may not be directly bound to selenos.

Selenos is found to interact with nsp7 in multiple interactome studies when nsp7 is used as a bait. Due to the central role of nsp7 in the replication of coronaviruses, we wondered whether selenos directly interacts with nsp7 and, if so, whether it competes or allows nsp7 to engage with its key protein partners in the RTC. Nsp7 and the nonstructural protein 8 (nsp8), serve as cofactors for the RNA-dependent RNA polymerase (RdRp, nsp12). Nsp12 catalyzes the RNA duplication from the viral RNA template, thus making it the very heart of the virus's replication machinery.[51–52] This complex is also responsible for the transcription of the viral proteins. Due to the central role of nsp12 in the replication of SARS-CoV-2, it has long been a target for designing antiviral drugs, such as molnupiravir. As mentioned, the nsp7/nsp8 complex vastly enhances the activity of nsp12.[53] These three proteins comprise the minimal complex required for RNA elongation.[54] Nsp7 is a conserved protein within the *Coronaviridae* family,[55] and mutations in nsp7 were found to hinder SARS-CoV-1 replication.[53] Accordingly, the virus is not viable without it.[56] In addition to its essential functions in the RTC, nsp7 has other cellular roles that are not well-understood. For example, a recent study on porcine epidemic diarrhea virus (PEDV) nsp7 reported that it inhibits the production of interferon type I.[57]

In the present study, we demonstrate that selenos interacts directly with nsp7 and not through a protein partner. We also determined whether this interaction competes with nsp8 binding or whether selenos can join the nsp7/nsp8 complex and even the coronavirus minimal RTC ((nsp7)$(nsp8)_2$(nsp12)). We have employed *in vitro* pull-down binding assays to characterize selenos interactions with the SARS-CoV-2 RTC proteins nsp7, nsp8, and nsp12. Through crosslinking experiments and mass spectrometry-based analysis, we have mapped which segment(s) of selenos are required for nsp7 binding and which are exposed and available for interactions with other protein partners even when selenos is bound to the RTC.

Results

To start, we tested whether nsp7 and selenos interact directly and, if so, whether these interactions depend on selenos's redox state and

thus the conformation of its C-terminal loop where the Sec resides (Figure 1). The Sec at position 188 forms a selenylsulfide bond with a Cys at position 174, thereby creating an internal loop at the C-terminus of selenos.[48–49] The formation or breakage of this selenylsulfide bond regulates the accessibility of Sec and allows it to react with substrates.[48–49] We designed *in vitro* pull-down assays using purified nsp7 and selenos. Although there are many unanswered questions regarding selenos's enzymatic use of its Sec, our work here investigates selenos's binding interactions with viral proteins and thus the presence of Sec is not essential. Since these interactions do not involve selenos's C-terminus (see below), we used throughout this study a variant of selenos in which the penultimate Sec had been exchanged with Cys. Employing this mutation (U188C) allows us to obtain homogenous protein samples, as the incorporation of Sec is mediated through the opal stop codon, and premature truncations can lead to sample heterogeneity.[58] The substitution introduces minimal structural perturbation as Sec and Cys are structurally similar amino acids.[59] In addition, we have previously shown that when Sec188 is substituted with Cys, the internal loop is still formed by a disulfide between Cys174 and Cys188.[48–49]

Selenos is positively charged at physiological pH, with a calculated isoelectric point (pI) of 9.7, and can on occasion electrostatically bind to chromatography resins. To minimize the nonspecific binding of the highly charged selenos to the resin, we carried out the pull-downs with StrepTactin resin. We employed nsp7 with a C-terminal strep-tag II (abbreviated as 'nsp7-strep') because, in structures of the RTC, the nsp7 C-terminus points away from the complex and is exposed to the solvent, rendering this terminus less likely to hinder protein interactions (Figure S1). Based on our previous characterization of selenos's behavior in different detergents, we chose the detergent n-dodecyl β-D-maltoside (DDM) to solubilize it.[60–62]

To demonstrate direct binding interactions, nsp7-strep was incubated with selenos U188C under reducing and non-reducing conditions. Nsp7-strep and bound proteins were subsequently isolated using StrepTactin resin (Figure 2(a,b)). Selenos U188C was bound to nsp7-strep, demonstrating that the interaction between nsp7 and selenos is direct and not mediated by a protein partner. Furthermore, the ratio of selenos U188C bound to nsp7-strep was similar under both reduceding and nonreducing conditions. Thus, the possibility that the interactions were due to an intermolecular disulfide bond was excluded. This also showed that binding was not impacted by the conformation of selenos's C-terminus. It should be noted that

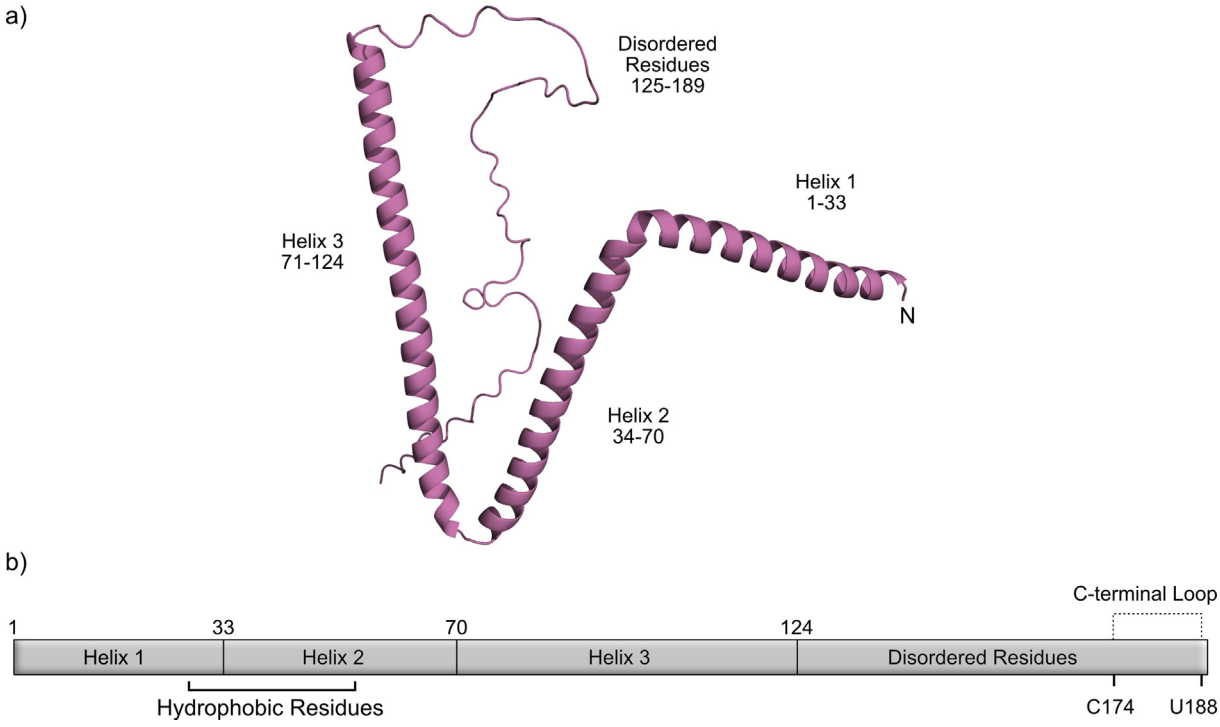

Figure 1. Structural model of selenos. a) The structural model of full-length selenos by AlphaFold2. b) The segmentation of selenos's secondary elements by AlphaFold2 consists of three helices (1–33, 34–70, and 73–124) and a disordered segment (125–189) that contains the enzymatic residues Cys174 and Sec188. They can form a loop in the C-terminus of selenos via a selenylsulfide bond. Residues 18 to 49 contain hydrophobic amino acids that are responsible for selenos's associations with membranes.

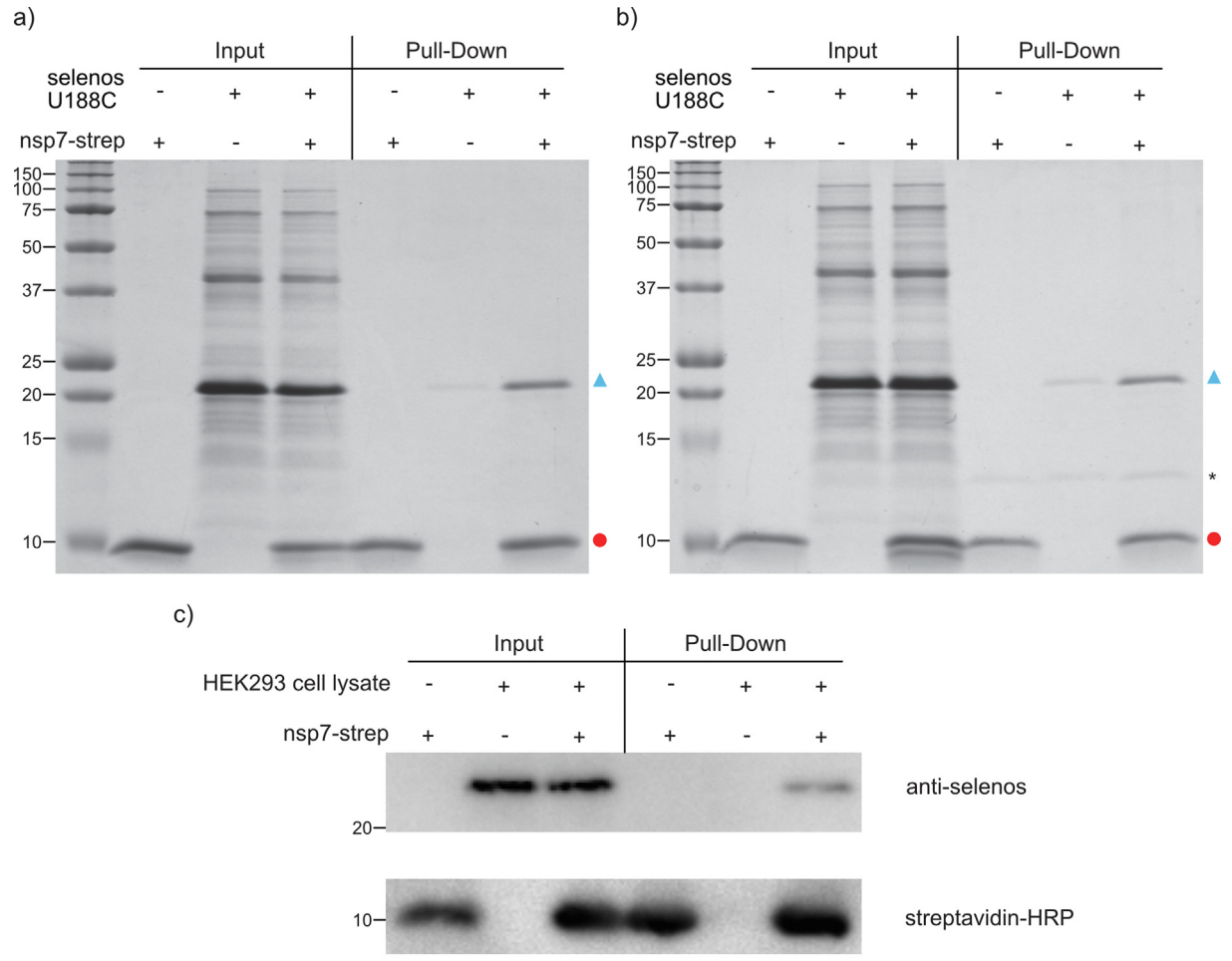

Figure 2. Pull-downs of selenos U188C as prey with nsp7-strep as bait. a) Tricine-SDS-PAGE of *in vitro* pull-down of selenos U188C with nsp7-strep under oxidizing conditions. Selenos is indicated with a cyan triangle, and nsp7-strep with a red circle. A weak selenos band can be seen in the control, which is due to electrostatic interactions with the column. b) Tricine-SDS-PAGE of the *in vitro* pull-down of selenos U188C with nsp7-strep under reducing conditions. The * marks a contamination due to StrepTactin resin that is only present only under reducing conditions. c) Western blot analysis of the pull-down of endogenous selenos from HEK293 lysates using purified nsp7-strep as bait.

the multiple bands observed in Tricine-SDS-PAGE of selenos are due to multimers of selenos, which are resistant to SDS denaturation. This observation is corroborated by size exclusion chromatography (Figure S2).

Nsp7 was reported to bind multiple human proteins,[36–42] many of which are abundant cellular proteins. However, selenos exhibits not only the low cellular abundancy typical for selenoproteins[63] but is also anchored to the membrane. Thus, we assessed selenos's ability to successfully compete with other nsp7 binding partners and achieve appreciable nsp7 binding in the presence of the competitors. These fundamental questions regarding binding of endogenous selenos to nsp7 were addressed via pull-down assays using HEK293 lysate and purified nsp7-strep. The results show that a considerable amount of endogenous selenos bound to nsp7-strep (Figure 2(c)).

Next, we narrowed down the segment of selenos required for interactions with nsp7. This is essential because selenos has multiple protein partners[50] and thus, to identify what role selenos plays in the virus life cycle, it is necessary to elucidate which segment(s) of selenos bind to nsp7 and which segment(s) remain free to bind to other protein partners. While the structure of full-length selenos remains unknown, it is often described as a single-pass transmembrane protein with residues 26–48 embedded into the ER membrane.[64] AlphaFold2[65] and RoseTTAFold[66–67] predict that selenos is divided into three α-helices: residues 1–33 (helix 1), 34–70 (helix 2), and 73–124 (helix 3). They are followed by a segment formed by residues 125–189 (Figure 1) that is rich in glycine, proline,

and polar residues and was confirmed to be unstructured by NMR studies.[68] This is also the segment that contains the reactive Sec at position 188. Therefore, we prepared a series of selenos variants with different residues to seek the segment(s) responsible for binding nsp7. In the first step, we split selenos into two segments. One consisted of residues 1 to 48 (N-terminus to the end of hydrophobic region) and thus contained helix 1. The other and the more soluble one, contained the remaining residues 48 to 189 and thus helix 3. However, the residues forming helix 2 were split between the two segments. Since these selenos segments were not equally stable, we studied them as fusion proteins with the maltose binding protein (MBP), which stabilized them. First, we performed a control experiment to establish that 6xHis-MBP does not interact with nsp7-strep under the selected experimental conditions (Figure S3), including the presence of DDM. Our control experiments indicated that nsp7-strep does not interact with 6xHis-MBP alone.

In our subsequent experiments looking at the binding of the two selenos segments, we found that there is no interaction between nsp7-strep and 6xHis-MBP-selenos 48–189 U188C (Figure S4(c)). In fact, within the sensitivity of the pull-down assays, the level of 6xHis-MBP-selenos 48–189 U188C bound to the StrepTactin resin was similar in the presence and absence of nsp7-strep. Likewise, the selenos variant with the N-terminus and hydrophobic segment, 6xHis-MBP-selenos 1–48, did not bind nsp7-strep (Figure S4 (b)). The observation that nsp7 binds to full-length selenos U188C but neither of its two segments suggested that the presence of only parts of helix 2 was insufficient for the binding interaction. Therefore, we next tested whether selenos's helix 2 (residues 34–70) is indeed the segment responsible for binding nsp7. Because helix 2 contains a hydrophobic portion (residues 35–48) as well as a stretch of four alanines and a valine (residues 66–70), we omitted these alanines and valine residues to help identify which hydrophobic residues contribute to binding. It was also already clear that the segment consisting of residues 48–70 alone, being part of a non-binding fragment, is insufficient for nsp7 binding. However, pull-down assay using a larger segment, 6xHis-MBP-selenos 34–65, indeed showed the helix 2 of selenos is sufficient for binding to nsp7-strep (Figure S4(d)). We then further segmented this stretch into three sections consisting of residues 34–59, 40–59, and 40–65 respectively. The results depicted in Figures 3 and S4(e,f) show that all three segments were able to bind nsp7-strep. However, any construct that was missing residues 40–59 was not able to bind. Thus, the segment containing residues 40–59 is both necessary and sufficient for binding nsp7. Unfortunately, quantitative measurements of the binding affinity were not feasible because—just like selenos—6xHis-MBP-selenos 40–59 also forms oligomers (see Figure S2), regardless if it was prepared with detergent or without it.

Nsp7 is part of the RTC but also acts as a transcription factor on its own.[43] Therefore, it may interact with selenos only when it is alone or part of the RTC. As these two possibilities have different biological ramifications, we expanded the *in vitro* studies to examine interactions with the nsp7/nsp8 complex. Here we performed the experiments using nsp7-strep, 6xHis-nsp8, and 6xHis-MBP-selenos U188C. The reason for choosing MBP-tagged selenos is because the molecular weight of 6xHis-nsp8 (22 kDa) is close to that of selenos (21 kDa), rendering quantification challenging by SDS-PAGE. We have already demonstrated (Figure S3) that the presence of MBP does not hinder the interaction of selenos with nsp7. For the pull-down assays, we incubated 6xHis-nsp8 with nsp7-strep and then added 6xHis-MBP-selenos U188C to the mixture. Both 6xHis-nsp8 and 6xHis-MBP-selenos U188C were coeluted from the StrepTactin resin only in the presence of nsp7-strep, demonstrating that the three proteins can form a complex (Figure 4). Additionally, we confirmed that 6xHis-nsp8 and selenos U188C do not interact strongly enough to survive *in vitro* pull-down conditions (Figure S5). Regradless if 6xHis-MBP-selenos U188C was present during the incubation of 6xHis-nsp8 with nsp7-strep or not, the intensities of the respective eluted 6xHis-nsp8 bands showed no significant differences. Thus, it appears that selenos does not compete with nsp8 for the nsp7 binding site.

Subsequently, we purified the minimal RTC ((nsp7)(nsp8)$_2$(nsp12)) and showed that it interacts with strep-selenos U188C (Figure 5). The three RTC proteins were co-expressed, and the complex was purified from *E. coli* following a procedure developed by Madru et al.[69] The minimal RTC purified using this procedure was previously shown to have the correct (nsp7)(nsp8)$_2$(nsp12) stoichiometry and to be active, i.e., to have RNA polymerization activity. The purified minimal RTC was incubated with strep-selenos U188C and isolated using StrepTactin resin (Figure 5). The complex was retained only when selenos was present, thereby unambiguously demonstrating that selenos can bind the minimal RTC.

To confirm the binding site on selenos and identify the nsp7 interaction site, we used crosslinking with the MS-cleavable disuccinimidyl sulfoxide (DSSO).[70–71] This cleavable crosslinker has two NHS ester groups that react with primary amine groups. Because the DSSO linker arm measures 10.3 Å when fully extended, it can crosslink lysines whose Cα atoms are as far 26.1 Å apart. Indeed, 90 % of experimentally observed distances fall below 27 Å.[72] Selenos has 16 lysines (Figure 6 (a)) including one at position 50, i.e., in the interacting region identified by the pull-downs (Figure 6(a)),

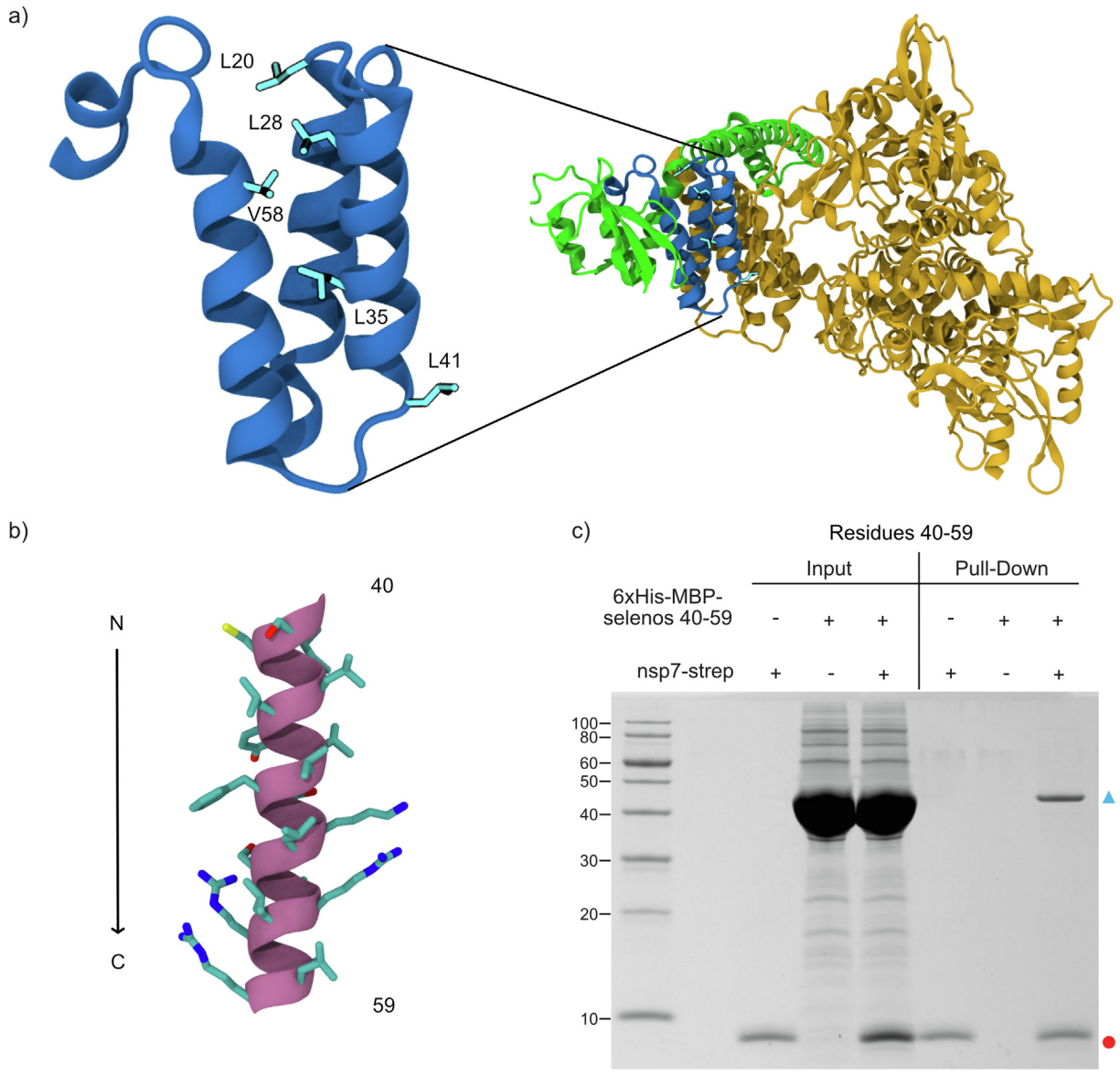

Figure 3. Identification of selenos residues required for nsp7 binding. a) Accessible surface-exposed hydrophobic residues when nsp7 is in complex with nsp8 and nsp12. A linear arrangement of surface exposed hydrophobic residues is present. b) The helix formed between residues 40–59 of selenos is also rich in hydrophobic residues. c) Tricine-SDS-PAGE of *in vitro* pull-down of 6xHis-MBP-selenos 40–59 with nsp7-strep under oxidizing conditions. 6xHis-MBP-selenos 40–59 is indicated with a cyan triangle, and nsp7-strep with a red circle.

while nsp7 has six lysines (Figure 6(b)). Because the strep-tag contains a lysine we utilized tagless nsp7 and selenos U188C for these experiments. To find a suitable crosslinker concentration and to minimize the possibility of unspecific crosslinking, we analyzed the disappearance of protein bands and the appearance of crosslinked bands with increasing concentrations of DSSO by SDS-PAGE (Figure S6). The best condition was identified as a 5:1 molar ratio of DSSO to total protein. Under these conditions, it is possible to visualize the complex formed between nsp7 and selenos U188C, but it accounts for less than 20 % of total protein. Following crosslinking, we chose to digest the crosslinked sample with the endoprotease α-lytic protease (aLP), which cleaves after threonine, alanine, serine, and valine. aLP was successfully able to digest the hydrophobic region of selenos's helix 2, which is resistant to trypsin digestion. Using a MS2-MS3 method, we mapped crosslinked lysine, serine, threonine, and tyrosine residues in the selenos/nsp7 complex (Figure 6(c)).

Of the six nsp7 lysine residues, we found that the ones crosslinked to selenos are Lys2 near the N-terminus, Lys27 on the second helix (residues 25–41) and Lys51 on the third helix (residues 45–61).

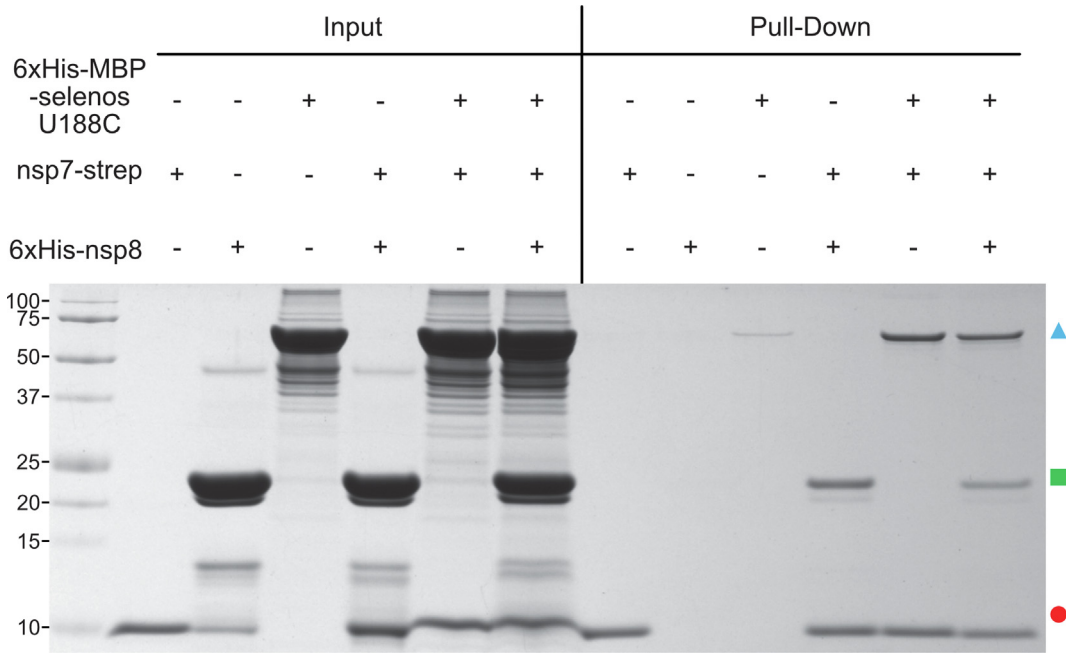

Figure 4. 6xHis-MBP-selenos U188C, nsp7-strep, and 6xHis-nsp8 form a ternary complex. Tricine-SDS-PAGE of *in vitro* pull-down of 6xHis-MBP-selenos U188C with 6xHis-nsp8 and nsp7-strep. 6xHis-MBP-selenos U188C is indicated with a cyan triangle, nsp7-strep with a red circle, and 6xHis-nsp8 with a green square.

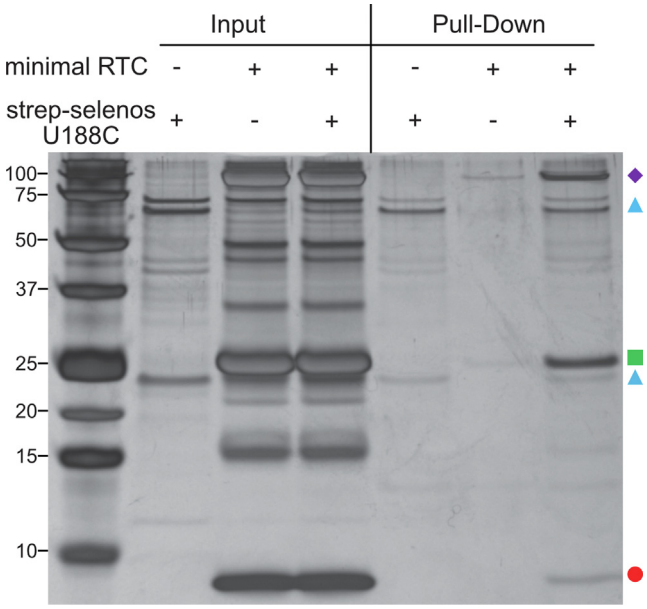

Figure 5. Pull-down of the minimal RTC using strep-selenos U188C. Components of the minimal RTC included nsp12 (purple rhombus), 14xHis-nsp8 (green square), and nsp7 (red circle) at a stoichiometry of 1:2:1. Selenos U188C (cyan triangle) interacted with the minimal RTC and can be seen in the pull-down eluate (right lane). The two bands marked with cyan triangles are different multimers of strep-selenos U188C.

All residues are exposed when nsp7 forms a complex with nsp8 and nsp12 (Figure 7). Nsp7 Lys27 and Lys51 were crosslinked to Lys77 and Lys88 of selenos, respectively (Figure 6(c)). Selenos Lys77 and Lys88 are located on its third helix, which in the structural model (Figure 1) is in the vicinity of selenos residues 40–59. Furthermore, Nsp7 Lys2 and Lys27 crosslink to the N-terminus of selenos and the hydroxyl of serine −1, a non-native residue that remains on selenos's N-terminus after 6xHis-MBP is removed by cleavage with TEV protease. Nsp7 Lys2 is

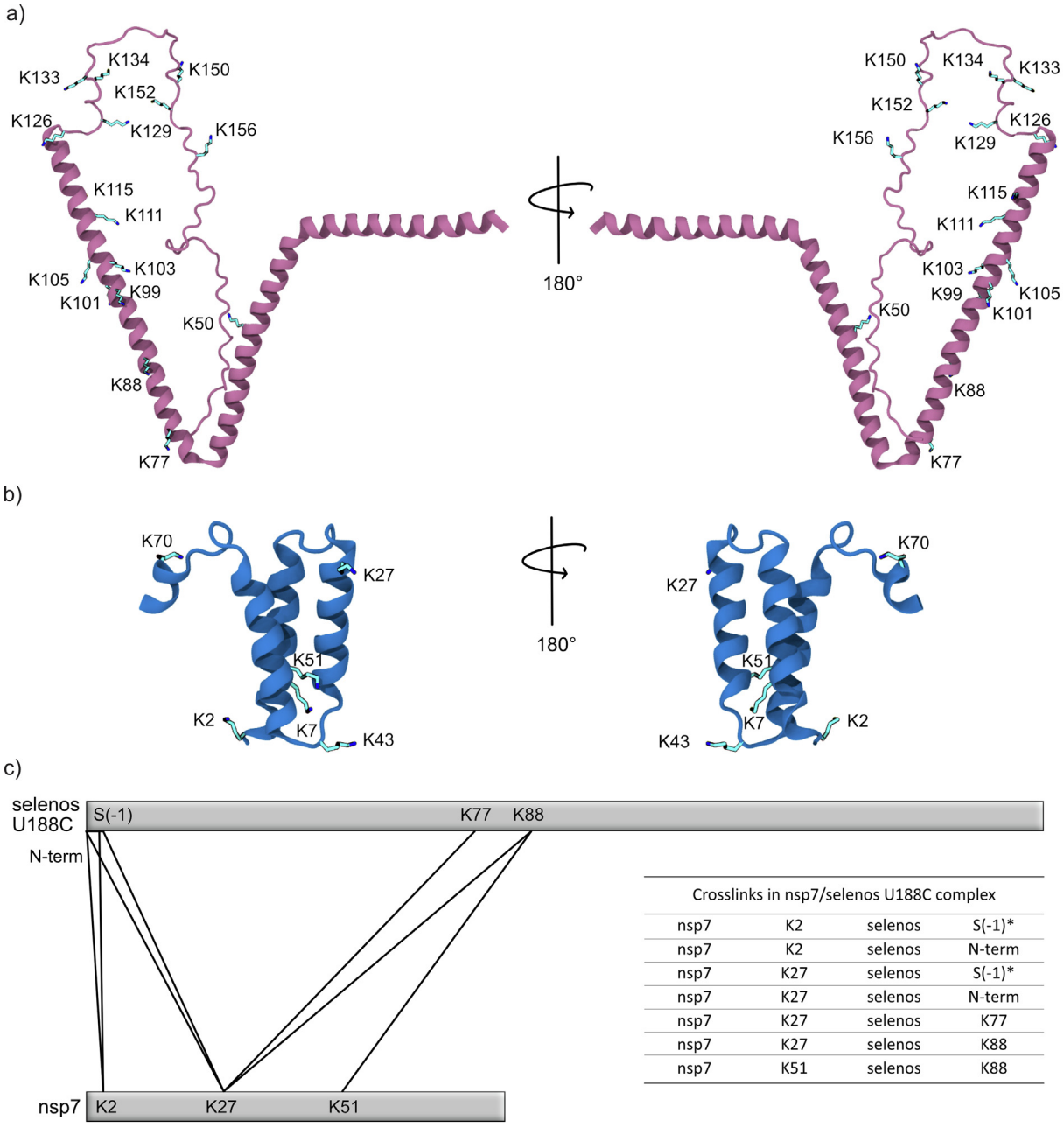

Crosslinks in nsp7/selenos U188C complex

nsp7	K2	selenos	S(-1)*
nsp7	K2	selenos	N-term
nsp7	K27	selenos	S(-1)*
nsp7	K27	selenos	N-term
nsp7	K27	selenos	K77
nsp7	K27	selenos	K88
nsp7	K51	selenos	K88

Figure 6. Crosslinking experiments between nsp7 and selenos U188C. a) Selenos's lysines are mapped onto the AlphaFold2 model. b) The location of all of lysines in nsp7 (nsp7 structure from PDB ID: 6XEZ). c) Crosslinks forming between selenos and nsp7 when they are in complex with each other. * S(-1) is a non-native residue that remains on selenos's N-terminus after purification.

located close to the loop between helix 2 and helix 3 and hence near the exposed surface of nsp7 in the minimal RTC (Figure 7). Selenos's helix 2 has only one lysine residue (Lys50), and it was not observed to form crosslinks with nsp7. It is probable that Lys50 interacts with nsp7 and thus is inaccessible in the nsp7/selenos complex.

Docking would lead to unreliable predictions because the experimental structure of full-length selenos is unavailable, and there are too few constraints avilable for the relevent segment due to the rarity of lysines on helix 2 and resulting crosslinks. Therefore, we analyzed the nsp7/nsp8/nsp12 complex and selenos's electrostatic surface potential using the Adaptive Poisson Boltzmann Solver (APBS) softer package (Figure 8). These calculations show a hydrophobic patch on the exposed surface of nsp7 in the nsp7/nsp8/nsp12 complex, which is mainly provided by nsp7 helix 2. This region is surrounded by charged surfaces contributed by nsp8 and nsp12. Selenos's helix 2 presents on one side a hydrophobic patch that

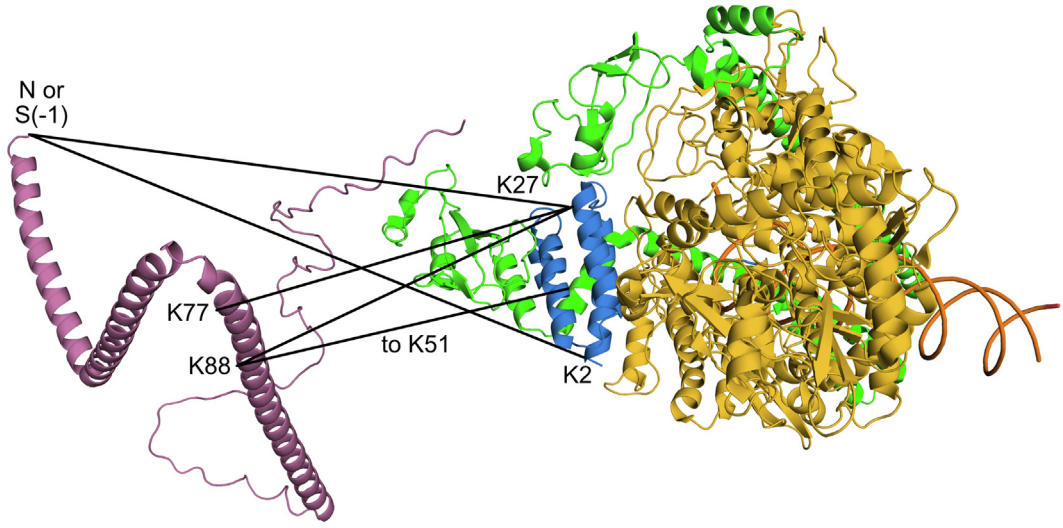

Figure 7. The crosslinks between selenos and nsp7 were mapped using the selenos AlphaFold2 model and RTC structure (PDB ID: 6XEZ; nsp13 not shown). The second helix of selenos binds to nsp7. However, because the number of lysines in helices 1 and 2 of selenos is low, most crosslinks are observed between its helix 3 and nsp7. Nsp12 is colored yellow, nsp7 is blue, nsp8 is green, and selenos is magenta.

can interface with nsp7. Charges on the other side can interact with those surrounding nsp7 and possibly enhance the binding affinity.

Discussion

Using *in vitro* pull-downs of purified proteins, we presented evidence that nsp7 and selenos bind directly. The interactions did not depend on the accessibility of cysteines or the conformation of selenos's C-terminal loop (Figure 2). Instead, they required selenos's helix 2 and a segment that at a minimum included the residues 40 to 59 (Figure 3). This is an unexpected finding, as selenos is believed to be an ER-resident type III membrane protein with a single transmembrane helix between residues 26 to 48.[73] Therefore, these residues are shielded by the membrane environment. In contrast, nsp7 is a soluble protein primarily located in the cytoplasm and nucleus.[74] Since selenos's helix 2, which contains many of these hydrophobic residues, is involved in binding to nsp7, interactions with nsp7 are only possible if part of selenos's helix 2 is exposed to the cytosol and not hidden in the membrane bilayer. Therefore, selenos may not be a transmembrane protein. Instead, it is possibly a monotopic membrane protein, i.e., it is attached to the cytoplasmic side of the ER membrane but does not cross it. Therefore, it is more likely that selenos helices 1 and 2 interact with one lipid leaflet, while helix 3 packs against them.

In addition to binding to nsp7, the pull-down assays confirmed that selenos also binds to the nsp7/nsp8 and the nsp7/nsp8/nsp12 complexes (Figures 4 and 5). Nonetheless, selenos does not bind to nsp8 itself strongly enough to be detected by pull-downs (Figure S5). The fact that selenos can interact with nsp7 alone and when nsp7 is bound to members of the RTC is notable since nsp7, nsp8, and nsp12 are also known to have functions other than replication, i.e., controlling host transcription and manipulating signaling pathways.[75,43,76] Therefore, the associations with nsp7 could have been related to nsp7-independent functions, sequestering selenos from one of its cellular activities, or taking over some of the selenos's protein partners. While this may still be the case, the observation that selenos and nsp7 can associate in the presence of other RTC members allows for the possibility that selenos also contributes to replication or to the coronavirus's evasion of the human immune system. Indeed, interactions between selenos and the RTC during replication were reported in cells infected with the betacoronavirus mouse hepatitis virus (MHV).[36]

We employed crosslinking experiments using the MS-cleavable crosslinker DSSO to map the interactions between selenos and nsp7 (Figure 6C, Tables S2 and S3). The crosslinks between selenos and nsp7 point to the surface formed between nsp7 helices 2 (residues 25–41) and 3 (residues 45–61) as the interaction surface. We observed that selenos Lys77 and Lys88 and its N-terminus formed crosslinks to nsp7 Lys27 and Lys51 (Figure 6). This demonstrates the proximity of selenos's helix 2 to the binding interface of selenos and nsp7. Lys 50, which is the only lysine in selenos's helix 2, may be shielded within the nsp7/selenos complex. Its N-terminus and the N-terminal serine forms crosslinks to nsp7 Lys27 and Lys2. Lys2 on the N-terminus of nsp7 is close to the second loop of nsp7 and exposed in the minimal RTC (Figure 8).

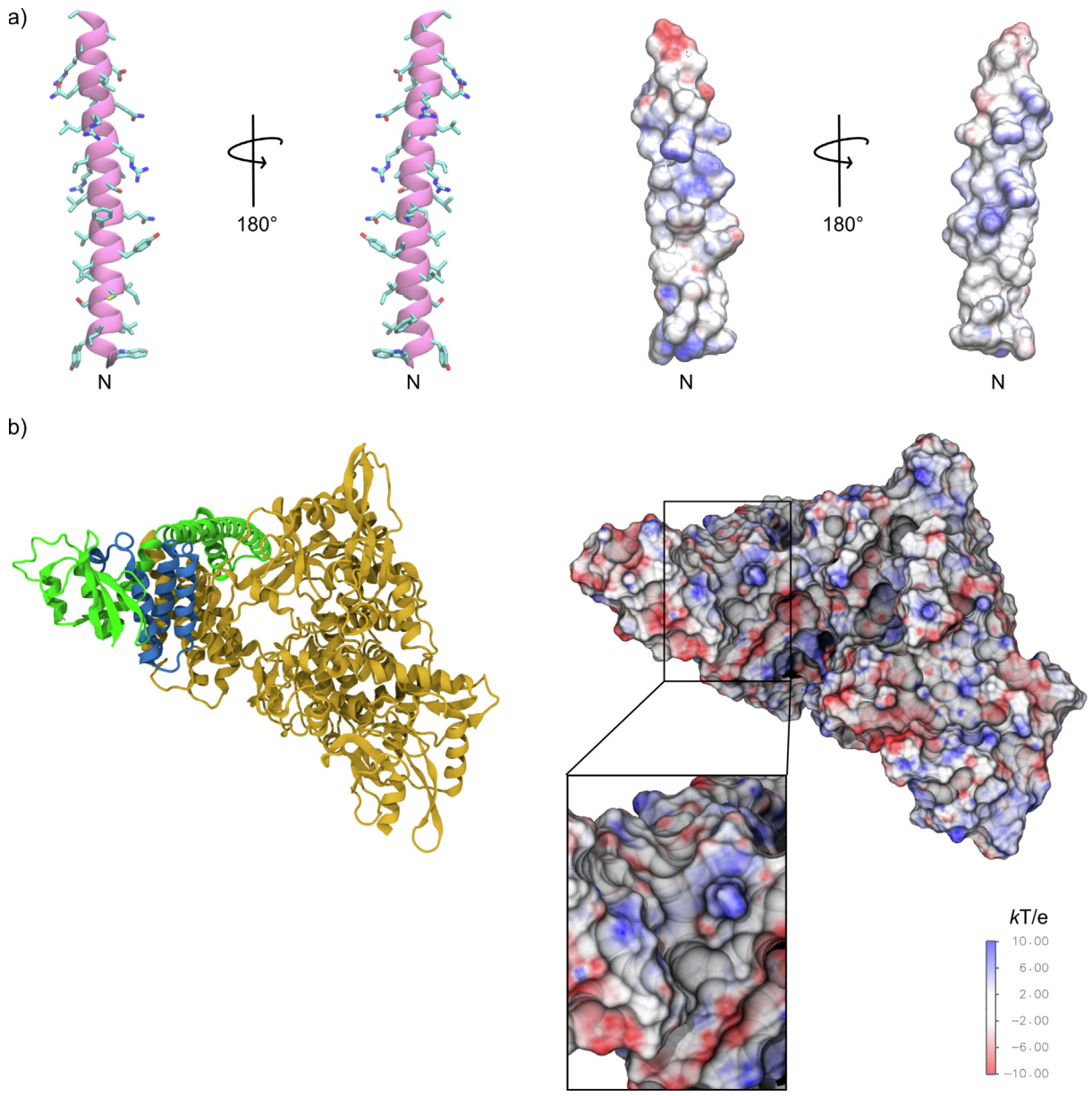

Figure 8. Complementary charges of selenos and the minimal RTC. a) View of the residues and surface potential of selenos's helix 2 displaying a hydrophobic patch near the N-terminus and positively charged residues in the middle. b) The electrostatic potential calculation of minimal RTC extracted from the structure of nsp7/nsp8/nsp12/nsp13/RNA (PDB ID: 6XEZ; nsp13 not shown). Nsp7 solvent-exposed surface contains hydrophobic and negatively charged patches. Nsp12 is colored yellow, nsp7 is blue, nsp8 is green, and selenos is magenta.

Because the N-terminus of selenos forms numerous internal crosslinks (Tables S2 and S3) it appears to be flexible.

Since a structure of full-length selenos is not available, a meaningful docking model cannot be generated. Indeed, a publication that reported docked selenos on nsp7, using the crystal structure of selenos's residues 52–122 (PDB 2Q2F, uncited entry), stated that selenos contacts nsp7 helix 1 and helix 2.[77] These helices are, in fact, shielded in the RTC by nsp12, and since we have shown that selenos can bind to the complex (Figure 5), the docking report does not agree with our findings reported here. Instead of docking, we have examined the electrostatics of the helices shown to be relevant for binding (Figure 8). Multiple structures are available for the RTC of SARS-CoV-2, in monomeric[78–82] and dimeric[83] forms of RdRp, with and without RNA and with accessory proteins. The cryo-EM structure that has the most components of the RTC structure to date—including nsp7/nsp8/nsp12/nsp13/RNA— is PDB ID

6XEZ.[78] Using this cryo-EM structure, we identified a surface exposed hydrophobic patch on nsp7 (see Figure 8 zoom) that is suitable for binding selenos's residues 40–59. This surface is exposed in all available cryo-EM structures of the RTC and the model of the entire replication complex proposed by Campbell et al.[84] We projected the crosslinks experimentally observed between selenos and nsp7 onto the RTC structure (Figure 7).

The role of selenos interactions with nsp7 alone, nsp7/nsp8, and the RTC remains unknown, however, we have shown that because nsp7 binds to selenos's helix 2, it is likely to disrupt selenos's interactions with protein partners in this segment. However, other components, such as the intrinsically disordered segment with the reactive Sec, will likely remain exposed and accessible to recruit additional proteins. Thus, SARS-CoV-2 may use selenos to recruit other proteins to interfere with cellular processes or to take them over for its replication.

Sequestration or exploitation of selenos by the coronavirus appears to be important because multiple reports of the SARS-CoV-2 interactome with human host proteins have identified interactions of selenos with coronavirus proteins (Table S1). Indeed, many viral and host proteins have multiple functions in assisting the coronavirus, and selenos may play more than one role in the virus's lifecycle. It may be that its enzymatic activity and/or its ability to recruit human proteins assists replication. Neither would be particularly unusual, as nonstructural proteins of coronaviruses rely on host proteins to assist with viral replication. For example, the EWSR1 (EWing Sarcoma breakpoint Region 1 / EWS RNA binding protein 1) helps the helicase nsp13 to unwind the viral RNA.[85] Alternatively, selenos was shown to inhibit the expression of inflammatory cytokines in CD4+ effector T cells (Teffs) by controlling the Ca^{2+}/NFATC2 signaling pathway and regulating the expression of the transcription factor E2F5.[13] In this way, the virus possibly controls these signaling pathways. Additionally, if selenos is deleted and thus cannot play its role in the ERAD, substrates of this degradation process accumulate. .[86] The virus may manipulate it to modify protein degradation. It may also be part of an assembly complex that— along with the viral nsp3, nsp4, and nsp6— generates the double membrane vesicles (DMVs). It is believed that using these structures aid the RTC in hiding from the immune system.[87] These viral proteins are also part of the central pore through which newly synthesized RNA is transferred.[46] Selenos also plays a role in the storage of lipids and fatty acids,[88–89] which is yet another cellular process that is modified by the virus in order to aid its own successful replication. Pinpointing the need to recruit selenos into the heart of the viral replication will be valuable for identifying the steps of viral replication and takeover of cellular pathways.

Materials and Methods

Materials

HEK-293 cells were from ATCC (CRL-1573). Dulbecco's Modified Eagle's Medium (DMEM) from Corning (#10–013-CV) was used for culturing human cells. For western blotting, anti-selenos (Invitrogen #MA5-31950) and secondary HRP conjugated antibody (Invitrogen #A16011) were used. For strep-tagged selenos, Precision Protein™ StrepTactin-HRP Conjugate (Bio-Rad #1610380) was utilized. StrepTactin resin was from IBA Lifesciences (#2–5010-025). Q5™ Site-Directed Mutagenesis Kit (#E0552S) from New England Biolabs (NEB) was used for mutagenesis. Primers were synthesized by Sigma-Aldrich. Protein sequences, expression plasmids and plasmid number for all proteins are provided in SI Table S4.

Expression and purification of selenos and its variants

Selenos U188C gene was cloned into the pMAL™-c5X vector (NEB) as previously described.[48,60] All mutations were confirmed by Sanger sequencing (AZENTA Life Sciences). Expression plasmids were transformed into *E. coli* strain C43(DE3). Colonies were transferred to LB medium (1 % (w/v) tryptone, 0.5 % (w/v) yeast extract, 0.5 % (w/v) NaCl and 100 μg/mL ampicillin) and incubated overnight at 37 °C, while shaking at 180 rpm. 10 mL of the seeding culture was transferred to 3 L flasks containing 1 L of TB medium (1.2 % (w/v) tryptone, 2.4 % (w/v) yeast extract, 0.4 % (v/v) glycerol, 17 mM potassium phosphate monobasic, 72 mM potassium phosphate dibasic, and 100 μg/mL ampicillin). Flasks were incubated at 37 °C, 180 rpm. At OD_{600} 0.6, the temperature decreased to 18 °C, and after 1 hour, the expression was induced with 0.3 mM Isopropyl β-D-1-thiogalactopyranoside (IPTG). After 18 hours, cells were harvested by centrifugation 4,225 × g for 15 minutes at 4 °C. Pellets were resuspended in lysis buffer (20 mM Tris.Cl pH 8.0, 300 mM NaCl, 30 mM imidazole, 0.1 mM EDTA), snap-frozen using liquid nitrogen and kept at −80 . For purification, pellets were thawed, 1 mM PMSF and 1 mM benzamidine hydrochloride added, and were broken using LM−10 Microfluidizer Processor. For full-length selenos and variants containing hydrophobic residues 0.6 mM DDM was added to the lysis buffer. Cell lysates were centrifuged at 30,000 × g for 30 minutes at 4 °C. The supernatant was loaded on 5 mL HisTrap FF (Cytiva) equilibrated with lysis buffer containing 0.5 mM DTT and washed with the same buffer. Proteins were eluted using the lysis buffer containing 500 mM imi-

dazole. The eluate was loaded on 60 mL amylose resin (NEB # E8021L) equilibrated with lysis buffer, and washed with the same buffer. Elution was done with lysis buffer containing 30 mM maltose. To remove the MBP, selenos U188C, the eluate was incubated overnight with TEV protease at a 40:1 molar ratio and loaded on 5 mL HisTrap FF to remove MBP and TEV protease. The flow-through was collected. The buffer for all samples was exchanged to 20 mM HEPES pH 7.4, 150 mM NaCl and 1 mM EDTA (and 0.6 mM DDM for variants containing hydrophobic residues) using HiPrep 26/10 desalting column (Cytiva). For crosslinking, selenos U188C was concentrated using Amicon® Ultra-15 Centrifugal Filters, and further purified on Superose 6 Increase 10/300 GL (Cytiva). Selenos purity was estimated to be above 95 % from Tricine-SDS-PAGE and intact protein mass spectrometry (Figure S2). Samples were used fresh or snap-frozen in liquid nitrogen and kept at −80 °C. The molecular weight of purified proteins was confirmed using intact protein mass spectrometry.

Nsp7 expression and purification

The expression vector for the C-terminal Strep II-tagged nsp7 (Addgene plasmid ID 145615) was transformed into BL21(DE3). Colonies were transferred to LB medium (1 % (w/v) tryptone, 0.5 % (w/v) yeast extract, 0.5 % (w/v) NaCl and 25 μg/mL chloramphenicol) and incubated overnight at 37 °C, 180 rpm. 10 mL of the seeding culture was transferred to 3 L flasks containing 1 L of TB medium (1.2 % (w/v) tryptone, 2.4 % (w/v) yeast extract, 0.4 % (v/v) glycerol, 17 mM potassium phosphate monobasic, 72 mM potassium phosphate dibasic, and 25 μg/mL chloramphenicol). Flasks were incubated at 37 °C while shaking at 180 rpm. At OD_{600} 0.6, the temperature decreased to 18 °C, and after 1 hour, the expression was induced with 0.5 mM IPTG. Cells were harvested by centrifugation 4,225 × g for 15 minutes at 4 °C. Pellets were resuspended in lysis buffer (50 mM Tris.Cl pH 8.0, 200 mM NaCl, 1 mM EDTA), snap-froze using liquid nitrogen, and kept at −80 °C. For purification, pellets were thawed, 1 mM PMSF and 1 mM benzamidine hydrochloride were added, and cells were lysed using LM−10 Microfluidizer Processor. Cell lysates were centrifuged at 30,000 × g for 30 minutes at 4 °C. The supernatant was loaded on 15 mL StrepTactin XT resin (IBA) equilibrated with lysis buffer and washed with the same buffer. The sample was loaded on Superdex 75 Increase 10/300 (Cytiva) equilibrated with 20 mM HEPES pH 7.4, 150 mM NaCl, 1 mM EDTA. Fractions containing nsp7-Strep were collected and concentrated using Amicon Ultra-15 Centrifugal Filters and were kept at −80 °C after snap-freezing with liquid nitrogen. To remove the affinity tag, the purified protein was incubated with TEV protease overnight at a molar ratio of 1:30. Then it was loaded on 15 mL StrepTactin XT resin (IBA) to remove tag and intact proteins. Then the sample was loaded on 5 mL HisTrap FF (Cytiva) to remove TEV protease. The buffer was exchanged to 20 mM HEPES pH 7.4, 150 mM NaCl and 1 mM EDTA using HiPrep 26/10 desalting column (Cytiva). The molecular weight of the purified nsp7 was confirmed using intact protein mass spectrometry.

Nsp8 expression and purification

Nsp8 gene, codon optimized for heterologous expression in *E. coli*, was cloned using Addgene plasmid ID 145595 into a pETDuet-1 expression vector. The resulting nsp8 construct had an N-terminus 6xHis tag and a TEV protease cleavage site. The expression plasmid was transformed into *E. coli* strain BL21 (DE3). Colonies were transferred to LB medium (1 % (w/v) tryptone, 1 % (w/v) yeast extract, 0.5 % (w/v) NaCl and 100 μg/mL ampicillin) and incubated overnight at 37 °C, 180 rpm. 10 mL of the seeding culture was transferred to 3 L flasks containing 1 L of TB medium (1.2 % (w/v) tryptone, 2.4 % (w/v) yeast extract, 0.4 % (v/v) glycerol, 17 mM potassium phosphate monobasic, 72 mM potassium phosphate dibasic, and 100 μg/mL ampicillin). Flasks were incubated at 37 °C while shaking at 180 rpm. At OD600 0.6, the temperature decreased to 18 °C, and after 1 hour, the expression was induced with 0.5 mM IPTG. Cells were harvested by centrifugation 4,225 × g for 15 minutes at 4 °C. Pellets were resuspended in lysis buffer (20 mM Tris.Cl pH 8.0, 200 mM NaCl, 10 mM imidazole, 0.5 mM EDTA), snap-frozen using liquid nitrogen and kept at −80 °C. For purification, pellets were thawed, and 1 mM PMSF and 1 mM benzamidine hydrochloride were added. Cells were lysed using a Microfluidics LM-10 Microfluidizer on ice, and all subsequent procedures were conducted at 4 °C. Cell lysates were centrifuged at 30,000 × g for 30 minutes at 4 °C. The supernatant was loaded on 5 mL HisTrap FF (Cytiva). The HisTrap column was equilibrated with lysis buffer and the protein eluted using 20 mM Tris.Cl pH 8.0, 200 mM NaCl, 500 mM imidazole, 0.5 mM EDTA. Following elution, the sample buffer was exchanged to 20 mM Tris.Cl pH 8.0, 100 mM NaCl, 1 mM EDTA by dialysis. The sample was loaded on Mono Q 10/10 (Cytiva) equilibrated with 20 mM Tris.Cl pH 8.0, 100 mM NaCl, 1 mM EDTA and eluted with gradient up to 1 M NaCl. Fractions containing 6xHis-nsp8 were collected, and the buffer was exchanged to 20 mM HEPES pH 7.4, 150 mM NaCl and 1 mM EDTA using HiPrep 26/10 desalting column (Cytiva). The sample was concentrated using Amicon Ultra-15 Centrifugal Filters and kept at −80 °C after snap-freezing with liquid nitrogen. The nsp8-strep construct was purified using the method explained for nsp7-

strep. The molecular weight of proteins was confirmed using intact protein mass spectrometry.

Expression and purification of the minimal replication and transcription complex

SARS-CoV-2 minimal RTC was prepared according to published procedures by the Delarue group,[69] using Addgene plasmid ID 165451. Nsp7 and nsp12 were tag-less, while nsp8 had an N-terminal 14xHis tag. Briefly, cells were lysed using a Microfluidics LM-10 Microfluidizer on ice, and all subsequent procedures were conducted at 4 °C. Cell lysates were centrifuged at 30,000 × g for 30 minutes at 4 °C. The supernatant was loaded on 5 mL HisTrap FF (Cytiva) equilibrated with 20 mM Tris.Cl pH 8.0, 300 mM NaCl, 25 mM imidazole, and washed with the same buffer. Elution was done using a gradient of 25 to 500 mM imidazole in the same buffer. After collecting the best fractions, the sample buffer was exchanged to 20 mM Tris.Cl pH 8.0, 150 mM NaCl, using HiPrep 26/10 desalting column (Cytiva). The sample was loaded on a 5 mL HiTrap Q column (Cytiva) equilibrated with 20 mM Tris.Cl pH 8.0. Fractions containing the complex were collected and concentrated using Amicon Ultra-15 Centrifugal Filters and loaded on Superose 6 Increase 10/300 GL (Cytiva) equilibrated with 20 mM HEPES pH 8.0, 150 mM NaCl, 1 mM $MgCl_2$. Best fractions were collected and were kept at −80 °C after snap-freezing with liquid nitrogen.

Pull-down assays

200 μL StrepTactin XT 4Flow resin was packed in Pierce Micro-Spin columns. The columns were equilibrated with loading buffer: 20 mM HEPES pH 7.4, 150 mM NaCl, and 0.3 mM DDM. Samples were mixed, and DDM concentration was adjusted to 0.3 mM and incubated for one hour at 4 °C. For all the selenos full-length and variants pull-downs, the molar ratio of selenos to nsp7-strep was set to a 4:1 molar ratio. For nsp7/nsp8/selenos pull down, first, 6xHis-nsp8 was added to nsp7-strep to a 4:1 molar ratio. After 1 hour, 6xHis-MBP-selenos U188C was added to the 4:1 molar ratio of nsp7-strep. For minimal RTC pull-downs, the molar ratio of strep-selenos to nsp7 was 1:4. Samples were loaded on columns and washed for 28 CV (column volume) of the loading buffer. The last two CV washes of the column were also examined by SDS-PAGE to assure column washing was sufficiently thorough. Bound proteins were eluted with 150 μL of the loading buffer supplemented with 50 mM biotin.

Cell culture and cell lysis

HEK293 cells were grown in DMEM medium (Corning #10–013-CV) containing 10 % fetal bovine serum (FBS) and 1 % penicillin–streptomycin supplemented with 60 nM sodium selenite. The cells were trypsinized, washed twice with cold PBS buffer, and lysed with cold lysis buffer (25 mM Tris-HCl pH 7.4, 150 mM NaCl, 1 % Ipegal, 1 mM EDTA, 5 % glycerol) supplemented with 10 μl/ml Halt Protease Inhibitor Cocktail (Thermo Scientific #78430). Cells were lysed on ice for one hour with periodic mixing and centrifuged at 18,000 × g for 10 minutes at 4 °C to pellet down the cell debris. The supernatant of the lysate was collected and analyzed by western blot.

Tricine-SDS-PAGE and western blotting

For Tricine-SDS-PAGE analysis, the sample mixed with 2x tricine loading buffer with 1 % 2-mercaptoethanol and 10 μL of each sample was loaded and resolved on a reducing 16 % Tricine-SDS-PAGE.[90] For western blotting, transfer was carried to a PVDF membrane at 20 V for 3 hours. The membrane was blocked with 5 % BSA in TBST (Tris-buffered saline, 0.1 % Tween 20) for 1 hour. Then was incubated with the primary antibody or 1 hour, washed three times, incubated with horseradish peroxidase (HRP) conjugated secondary antibody for 1 hour, and washed three times. The western blot was visualized using a chemiluminescent HRP substrate kit (Thermo Scientific #34075).

Crosslinking

10 μM of each protein in crosslinking buffer: 20 mM HEPES, pH 7.4, 150 mM NaCl, 1 mM EDTA (and 0.6 mM DDM for the fragments containing the hydrophobic residues) was prepared in a final volume of 100 μL and incubated for one hour at 4 °C. 2 μL of DSSO (Sigma-Aldrich #909602) in DMSO (freshly prepared) was added to a final concentration of 5 times molar ratio of the protein mixture and the sample incubated at 25 °C for 45 minutes. For controls, the mixture of the proteins was mixed with 2 μL DMSO. 1 M Tris.Cl, pH 8.0 buffer was added to a final concentration of 50 mM to quench the crosslinking for 15 minutes at 25 °C. 10 μL of the sample was saved for analysis by SDS-PAGE. 400 μL cold acetone was added to the remaining volume and was incubated on ice for one hour and centrifuged for 10 minutes at 20,000 × g. The supernatant was removed, and the samples were incubated for 30 minutes at room temperature to dry the precipitates. 12.5 μL of 50 mM sodium bicarbonate buffer, 8 M urea was used to resuspend the precipitate. 187.5 μL of 50 mM sodium bicarbonate was added to lower the urea concentration to 500 mM. DTT was added to a final concentration of 5 mM and the samples were incubated at 56 °C for 20 minutes. Afterward, iodoacetamide was added to a final concentration of 15 mM and the sample was incubated for 15 minutes in the dark. α-lytic protease (NEB # P8113S) was added to a 1:20 molar ratio and

incubated at 37 °C for 20 hours. Trifluoroacetic acid (TFA) was added to a final concentration of 1 % in the samples, and the peptides were purified using Pierce C18 tips (#87784). Peptides were dried using SpeedVac and stored at −20 °C until analysis by mass spectrometry. All crosslinking reactions and controls were performed in at least three independent reactions.

Liquid chromatography and mass spectrometry

For LC-MS/MS analysis, an Ultimate 3000 RSLCnano system coupled to an Eclipse Orbitrap mass spectrometer via a FLEX nano-electrospray source and a FAIMS Pro Interface (all from Thermo Scientific) were employed. Proteins derived from three biological replicates were used for three injections. The peptides were resuspended in (25 μl) LC solvent A (0.1 % formic acid in water) and (10 μL) first loaded onto a trap column (PepMap100 C18, 300 μm × 2 mm, 5 μm; Thermo Scientific) followed by separation on an analytical column (PepMap100 C18, 25 cm length, 75 μm i.d., 3 μm; Thermo Scientific). A linear LC gradient with a flow rate of 300 nL/min was applied from 1 % solvent B (0.1 % formic acid in acetonitrile) to 25 % solvent B (0.1 % formic acid in acetonitrile) over 125 minutes, followed by a steeper gradient to 32 % solvent B over 10 minutes. The column was washed with 95 % solvent B for 5 minutes, followed by equilibration with solvent A for 15 minutes. For the ion source settings, the spray voltage was set to 1.8 kV, funnel RF level at 30 %, and heated capillary temperature at 275 °C. MS data were acquired in data-dependent mode with three FAIMS compensation voltages (CVs), including −50, −60, and −75. The resolutions were set to 120,000 at m/z 200, the mass range was 375–1600, the AGC target was standard, and the maximum injection time mode was set to Auto. For MS2 analysis, precursors with charge states 2–8 were selected. The isolation mode was Quadrupole, the activation type was CID, and its collision energy was 25 %. Orbitrap was set to detect MS2 fragments at a resolution of 60,000 with a standard AGC target, 118 ms maximum injection time, and an isolation window of 1.6 m/z. For MS-cleavable linkers, a data-dependent MS3 method was applied. For reporter doublets, the targeted mass difference was set to 31.9721 Da, charge state to 1–6, and mass tolerance to ± 10 ppm. The selected MS3 scans were recorded using HCD fragmentation with 30 % collision energy in the ion trap, which was in rapid mode. The AGC target was 300 %, the maximum injection time was 150 ms, and the isolation window was set to 2 m/z for MS2 and 2.5 m/z for MS.

Crosslinking data analysis

Raw files were analyzed using Proteome Discoverer 2.5 and XlinkX 2.5 node. An MS2_MS3 workflow was set up with MS1 mass tolerance, 10 ppm; MS2 mass tolerance, 20 ppm; MS3 mass tolerance, 0.5 Da. Digestion was set to α-lytic protease (cleavage after T/A/S/V) with four missed cleavages allowed. The minimum peptide length was 4 amino acids. A static modification was carbamidomethylation of cysteine, and dynamic modification was oxidation of methionine and DSSO for lysines. The XlinkX/PD Validator node was used for crosslinked peptide validation with a 1 % false discovery rate (FDR). Crosslinks were examined manually and an XlinkX Score cutoff of 50 and a ΔXlinkX Score cutoff of 10 were considered as indicative of true crosslinks.

Intact mass spectrometry

Mass spectra of intact proteins were obtained using a Xevo G2-S QTOF on a Waters ACQUITY UPLC Protein BEH C4 reverse-phase column (300 A, 1.7 μm, 2.1 mm × 50 mm). An acetonitrile gradient from 5 %-95 % was used with 0.1 % formic acid, over a run time of 5 min and a constant flow rate of 0.5 mL/min at 40 °C. The spectra were deconvoluted using MaxEnt1.

Electrostatic surface potential calculation

The electrostatic surface potential of the RTC (PDB ID: 6XEZ) and helix 2 of selenos from an AlphaFold2 model was calculated using the Adaptive Poisson Boltzmann Solver (APBS) software package. For the case of the RTC, only chains A, B, and C were used to represent nsp7, nsp8, and nsp12, respectively. The surface potential was calculated with the linearized Poisson-Boltzmann equation, using a dielectric constant of 78.54 and a temperature of 278 K. In addition, the grid length was adjusted according to the molecular sizes of each of the proteins. The potential surface isocontour is scaled at ± 10 kT/e, displaying the positive and the negative charges in blue and red, respectively. Figures are visualized and rendered using Visual Molecular dynamics (VMD).[91–92]

CRediT authorship contribution statement

Farid Ghelichkhani: Conceptualization, Data curation, Methodology, Visualization. **Fabio A. Gonzalez:** Software, Visualization. **Mariia A. Kapitonova:** . **Sharon Rozovsky:** Conceptualization, Funding acquisition, Project administration, Resources, Supervision.

DATA AVAILABILITY

The mass spectrometry proteomics data have been deposited to the ProteomeXchange Consortium (http://

www.proteomexchange.org) via the PRIDE partner repository with the dataset identifier PXD038629.

Acknowledgments

Research reported in this publication was supported by the National Institute of General Medical Sciences of the National Institutes of Health under award number GM121607 and the National Science Foundation under Grant MCB-2150863. FG was partly supported by the University of Delaware Graduate College Doctoral Fellowship Award. We thank the Mass Spectrometry Facility in the University of Delaware for assistance, which is supported by National Institute of General Medical Sciences Award Number P20GM104316.

Declaration of Competing Interest

The authors declare that they have no known competing financial interests or personal relationships that could have appeared to influence the work reported in this paper.

Appendix A. Supplementary data

Supplementary data to this article can be found online at https://doi.org/10.1016/j.jmb.2023.168008.

Received 4 August 2022;
Accepted 3 February 2023;
Available online 10 February 2023

Keywords:
Selenos;
Sels;
Nsp8;
Nsp12;
VIMP

References

1. Schomburg, L., (2022). Selenium Deficiency in COVID-19—A Possible Long-Lasting Toxic Relationship. *Nutrients* **14**, 283. https://doi.org/10.3390/nu14020283.
2. Golin, A., Tinkov, A.A., Aschner, M., Farina, M., da Rocha, J.B.T., (2023). Relationship between selenium status, selenoproteins and COVID-19 and other inflammatory diseases: A critical review. *J. Trace Elem. Med Biol.* **75**, https://doi.org/10.1016/j.jtemb.2022.127099 127099.
3. Hatfield, D.L., Tsuji, P.A., Carlson, B.A., Gladyshev, V.N., (2014). Selenium and selenocysteine: Roles in cancer, health, and development. *Trends Biochem. Sci* **39**, 112–120. https://doi.org/10.1016/j.tibs.2013.12.007.
4. Labunskyy, V.M., Hatfield, D.L., Gladyshev, V.N., (2014). Selenoproteins: Molecular pathways and physiological roles. *Physiol. Rev.* **94**, 739–777. https://doi.org/10.1152/physrev.00039.2013.
5. Santesmasses, D., Gladyshev, V.N., (2021). Pathogenic Variants in Selenoproteins and Selenocysteine Biosynthesis Machinery. *Int. J. Mol. Sci.* **22**, 11593. https://doi.org/10.3390/ijms222111593.
6. Khatiwada, S., Subedi, A., (2019). A Mechanistic Link Between Selenium and Coronavirus Disease 2019 (COVID-19). *Curr. Nutre Rep.* **10** (2021), 125–136. https://doi.org/10.1007/s13668-021-00354-4.
7. Brigelius-Flohé, R., Maiorino, M., (2013). Glutathione peroxidases. *BBA – General Subjects* **1830**, 3289–3303. https://doi.org/10.1016/j.bbagen.2012.11.020.
8. Ma, C., Hoffmann, F.W., Marciel, M.P., Page, K.E., Williams-Aduja, M.A., Akana, E.N.L., Gojanovich, G.S., Gerschenson, M., et al., (2021). Upregulated ethanolamine phospholipid synthesis via selenoprotein I is required for effective metabolic reprogramming during T cell activation. *Mol Metab.* **47**, https://doi.org/10.1016/j.molmet.2021.101170 101170.
9. Yim, S.H., Everley, R.A., Schildberg, F.A., Lee, S.-G., Orsi, A., Barbati, Z.R., Karatepe, K., Fomenko, D.E., et al., (2018). Role of Selenof as a Gatekeeper of Secreted Disulfide-Rich Glycoproteins. *Cell Rep.* **23**, 1387–1398. https://doi.org/10.1016/j.celrep.2018.04.009.
10. Fredericks, G.J., Hoffmann, F.W., Hondal, R.J., Rozovsky, S., Urschitz, J., Hoffmann, P.R., (2017). Selenoprotein K Increases Efficiency of DHHC6 Catalyzed Protein Palmitoylation by Stabilizing the Acyl-DHHC6 Intermediate. *Antioxidants (Basel).* **7** https://doi.org/10.3390/antiox7010004.
11. Lilley, B.N., Ploegh, H.L., (2005). Multiprotein complexes that link dislocation, ubiquitination, and extraction of misfolded proteins from the endoplasmic reticulum membrane. *PNAS* **102**, 14296–14301. https://doi.org/10.1073/pnas.0505014102.
12. Ye, Y.H., Shibata, Y., Yun, C., Ron, D., Rapoport, T. A., (2004). A membrane protein complex mediates retro-translocation from the ER lumen into the cytosol. *Nature* **429**, 841–847. https://doi.org/10.1038/nature02656.
13. Capelle, C.M., Zeng, N., Danileviciute, E., Rodrigues, S.F., Ollert, M., Balling, R., He, F.Q., (2021). Identification of VIMP as a gene inhibiting cytokine production in human CD4+ effector T cells. *IScience.* **24**, https://doi.org/10.1016/j.isci.2021.102289 102289.
14. Ghelichkhani, F., Gonzalez, F.A., Kapitonova, M.A., Schaefer-Ramadan, S., Liu, J., Cheng, R., Rozovsky, S., (2022). Selenoprotein S: A versatile disordered protein. *Arch. Biochem. Biophys.* **731**, https://doi.org/10.1016/j.abb.2022.109427 109427.
15. Liu, J., Rozovsky, S., (2015). Membrane-bound selenoproteins. *Antioxid. Redox Signal.* **23**, 795–813. https://doi.org/10.1089/ars.2015.6388.
16. Addinsall, A.B., Wright, C.R., Andrikopoulos, S., van der Poel, C., Stupka, N., (2018). Emerging roles of endoplasmic reticulum-resident selenoproteins in the regulation of cellular stress responses and the implications for metabolic disease. *Biochem. J* **475**, 1037–1057. https://doi.org/10.1042/bcj20170920.
17. Alanne, M., Kristiansson, K., Auro, K., Silander, K., Kuulasmaa, K., Peltonen, L., Salomaa, V., Perola, M., (2007). Variation in the selenoprotein S gene locus is associated with coronary heart disease and ischemic

stroke in two independent Finnish cohorts. *Hum. Genet.* **122**, 355–365. https://doi.org/10.1007/s00439-007-0402-7.
18. Strauss, E., Tomczak, J., Staniszewski, R., Oszkinis, G., (2018). Associations and interactions between variants in selenoprotein genes, selenoprotein levels and the development of abdominal aortic aneurysm, peripheral arterial disease, and heart failure. *PLoS One* **13**, e0203350.
19. Sutherland, A., Kim, D.H., Relton, C., Ahn, Y.O., Hesketh, J., (2010). Polymorphisms in the selenoprotein S and 15-kDa selenoprotein genes are associated with altered susceptibility to colorectal cancer. *Genes Nutr.* **5**, 215–223. https://doi.org/10.1007/s12263-010-0176-8.
20. Meplan, C., Hughes, D.J., Pardini, B., Naccarati, A., Soucek, P., Vodickova, L., Hlavata, I., Vrana, D., et al., (2010). Genetic variants in selenoprotein genes increase risk of colorectal cancer. *Carcinogenesis* **31**, 1074–1079. https://doi.org/10.1093/carcin/bgq076.
21. Mukhtar, M., Ashfield, N., Vodickova, L., Vymetalkova, V., Levy, M., Liska, V., Bruha, J., Bendova, P., et al., (2022). The Associations of Selenoprotein Genetic Variants with the Risks of Colorectal Adenoma and Colorectal Cancer: Case-Control Studies in Irish and Czech Populations. *Nutrients* **14**, 2718. https://doi.org/10.3390/nu14132718.
22. Gao, Y., Walder, K., Sunderland, T., Kantham, L., Feng, H. C., Quick, M., Bishara, N., de Silva, A., et al., (2003). Elevation in Tanis expression alters glucose metabolism and insulin sensitivity in H4IIE cells. *Diabetes* **52**, 929–934. https://doi.org/10.2337/diabetes.52.4.929.
23. Qiao, L., Men, L., Yu, S., Yao, J., Li, Y., Wang, M., Yu, Y., Wang, N., et al., (2022). Hepatic deficiency of selenoprotein S exacerbates hepatic steatosis and insulin resistance. *Cell Death Dis.* **13**, 275. https://doi.org/10.1038/s41419-022-04716-w.
24. Karlsson, H.K.R., Tsuchida, H., Lake, S., Koistinen, H.A., Krook, A., (2004). Relationship between serum amyloid A level and Tanis/SelS mRNA expression in skeletal muscle and adipose tissue from healthy and type 2 diabetic subjects. *Diabetes* **53**, 1424–1428. https://doi.org/10.2337/diabetes.53.6.1424.
25. Olsson, M., Olsson, B., Jacobson, P., Thelle, D.S., Björkegren, J., Walley, A., Froguel, P., Carlsson, L.M., et al., (2011). Expression of the selenoprotein S (SELS) gene in subcutaneous adipose tissue and SELS genotype are associated with metabolic risk factors. *Metabolism* **60**, 114–120. https://doi.org/10.1016/j.metabol.2010.05.011.
26. Li, F., Mao, A., Fu, X., She, Y., Wei, X., (2019). Correlation between SEPS1 gene polymorphism and type 2 diabetes mellitus: A preliminary study. *J. Clin. Lab. Anal.* **33**, e22967.
27. Zhao, L., Zheng, Y.Y., Chen, Y., Ma, Y.T., Yang, Y.N., Li, X.M., Ma, X., Xie, X., (2018). Association of genetic polymorphisms of SelS with Type 2 diabetes in a Chinese population. *Biosci. Rep.* **38** https://doi.org/10.1042/bsr20181696.
28. Gao, Y., Xie, X., Ma, Y.-T., Yang, Y.-N., Li, X.-M., Fu, Z.-Y., Zheng, Y.-Y., Ma, X., et al., (2013). Genetic variation in Tanis was associated with elevating plasma triglyceride level in Chinese nondiabetic subjects. *Lipids Health Dis.* **12**, 97. https://doi.org/10.1186/1476-511X-12-97.
29. Wang, T., Wang, B., Huang, H., Zhang, C., Zhu, Y., Pei, B., Cheng, C., Sun, L., et al., (2017). Enterovirus 71 protease 2Apro and 3Cpro differentially inhibit the cellular endoplasmic reticulum-associated degradation (ERAD) pathway via distinct mechanisms, and enterovirus 71 hijacks ERAD component p97 to promote its replication. *PLoS Pathog.* **13**, e1006674.
30. Liu, X., Palaniyandi, S., Zhu, I., Tang, J., Li, W., Wu, X., Ochsner, S.P., Pauza, C.D., et al., (2019). Human cytomegalovirus evades antibody-mediated immunity through endoplasmic reticulum-associated degradation of the FcRn receptor. *Nature Commun.* **10**, 3020. https://doi.org/10.1038/s41467-019-10865-y.
31. Wang, Y., Huang, J., Sun, Y., Stubbs, D., He, J., Li, W., Wang, F., Liu, Z., et al., (2021). SARS-CoV-2 suppresses mRNA expression of selenoproteins associated with ferroptosis, endoplasmic reticulum stress and DNA synthesis. *Food Chem. Toxicol.* **153**, https://doi.org/10.1016/j.fct.2021.112286 112286.
32. Bubenik, J.L., Miniard, A.C., Driscoll, D.M., (2013). Alternative transcripts and 3'UTR elements govern the incorporation of selenocysteine into selenoprotein S. *PLoS One* **8**, e62102–e. https://doi.org/10.1371/journal.pone.0062102.
33. Movaqar, A., Yaghoubi, A., Rezaee, S.R., Jamehdar, S.A., Soleimanpour, S., (2021). Coronaviruses construct an interconnection way with ERAD and autophagy. *Future Microbiol.* **16**, 1135–1151. https://doi.org/10.2217/fmb-2021-0044.
34. Wong, H.H., Kumar, P., Tay, F.P., Moreau, D., Liu, D.X., Bard, F., (2015). Genome-Wide Screen Reveals Valosin-Containing Protein Requirement for Coronavirus Exit from Endosomes. *J. Virol.* **89**, 11116–11128. https://doi.org/10.1128/jvi.01360-15.
35. Das, P., Dudley, J.P., (2021). How Viruses Use the VCP/p97 ATPase Molecular Machine. *Life Sci.* https://doi.org/10.20944/preprints202108.0542.v1.
36. V'kovski, P., Gerber, M., Kelly, J., Pfaender, S., Ebert, N., Lagache, S.B., Simillion, C., Portmann, J., et al., (2019). Determination of host proteins composing the microenvironment of coronavirus replicase complexes by proximity-labeling. *ELife* **8**, e42037.
37. Gordon, D.E., Hiatt, J., Bouhaddou, M., Rezelj, V.V., Ulferts, S., Braberg, H., Jureka, A.S., Obernier, K., et al., (2020). Comparative host-coronavirus protein interaction networks reveal pan-viral disease mechanisms. *Science* **370** https://doi.org/10.1126/science.abe9403.
38. Gordon, D.E., Jang, G.M., Bouhaddou, M., Xu, J., Obernier, K., White, K.M., O'Meara, M.J., Rezelj, V.V., et al., (2020). A SARS-CoV-2 protein interaction map reveals targets for drug repurposing. *Nature* **583**, 459–468. https://doi.org/10.1038/s41586-020-2286-9.
39. Stukalov, A., Girault, V., Grass, V., Karayel, O., Bergant, V., Urban, C., Haas, D.A., Huang, Y., et al., (2021). Multilevel proteomics reveals host perturbations by SARS-CoV-2 and SARS-CoV. *Nature* **594**, 246–252. https://doi.org/10.1038/s41586-021-03493-4.
40. Liu, X., Huuskonen, S., Laitinen, T., Redchuk, T., Bogacheva, M., Salokas, K., Pöhner, I., Öhman, T., et al., (2021). SARS-CoV-2-host proteome interactions for antiviral drug discovery. *Mol. Syst. Biol.* **17**, e10396 https://doi.org/10.15252/msb.202110396.
41. Laurent, E. M., Sofianatos, Y., Komarova, A., Gimeno, J. -P., Tehrani, P. S., Kim, D. -K., Abdouni, H., Duhamel, M., et al. (n.d.). Global BioID-based SARS-CoV-2 proteins proximal interactome unveils novel ties between viral polypeptides and host factors involved in multiple

COVID19-associated mechanisms. https://doi.org/10.1101/2020.08.28.272955.
42. Zhou, Y., Liu, Y., Gupta, S., Paramo, M.I., Hou, Y., Mao, C., Luo, Y., Judd, J., et al., (2022). A comprehensive SARS-CoV-2–human protein–protein interactome reveals COVID-19 pathobiology and potential host therapeutic targets. *Nature Biotechnol.*. https://doi.org/10.1038/s41587-022-01474-0.
43. Banerjee, A.K., Blanco, M.R., Bruce, E.A., Honson, D.D., Chen, L.M., Chow, A., Bhat, P., Ollikainen, N., et al., (2020). SARS-CoV-2 disrupts splicing, translation, and protein trafficking to suppress host defenses. *Cell* **183**, 1325–1339.e21. https://doi.org/10.1016/j.cell.2020.10.004.
44. Oh, S.-J., Shin, O.S., (2022). SARS-CoV-2-mediated evasion strategies for antiviral interferon pathways. *J. Microbiol.* **60**, 290–299. https://doi.org/10.1007/s12275-022-1525-1.
45. May, D. G., Martin-Sancho, L., Anschau, V., Liu, S., Chrisopulos, R. J., Scott, K. L., Halfmann, C. T., Peña, R. D. et al. (n.d.). A BioID-derived proximity interactome for SARS-CoV-2 proteins. https://doi.org/10.1101/2021.09.17.460814.
46. Wolff, G., Limpens, R., Zevenhoven-Dobbe, J.C., Laugks, U., Zheng, S., de Jong, A.W.M., Koning, R.I., Agard, D.A., et al., (2020). A molecular pore spans the double membrane of the coronavirus replication organelle. *Science* **369**, 1395–1398. https://doi.org/10.1126/science.abd3629.
47. Daniloski, Z., Jordan, T.X., Wessels, H.-H., Hoagland, D. A., Kasela, S., Legut, M., Maniatis, S., Mimitou, E.P., et al., (2021). Identification of required host factors for SARS-CoV-2 infection in human cells. *Cell* **184**, 92–105.e16. https://doi.org/10.1016/j.cell.2020.10.030.
48. Liu, J., Li, F., Rozovsky, S., (2013). The intrinsically disordered membrane protein selenoprotein S is a reductase in vitro. *Biochemistry* **52**, 3051–3061. https://doi.org/10.1021/bi4001358.
49. Liu, J., Rozovsky, S., (2013). Contribution of selenocysteine to the peroxidase activity of selenoprotein S. *Biochemistry* **52**, 5514–5516. https://doi.org/10.1021/bi400741c.
50. Turanov, A.A., Shchedrina, V.A., Everley, R.A., Lobanov, A.V., Yim, S.H., Marino, S.M., Gygi, S.P., Hatfield, D.L., et al., (2014). Selenoprotein S is involved in maintenance and transport of multiprotein complexes. *Biochem. J* **462**, 555–565. https://doi.org/10.1042/bj20140076.
51. Malone, B., Urakova, N., Snijder, E.J., Campbell, E.A., (2022). Structures and functions of coronavirus replication–transcription complexes and their relevance for SARS-CoV-2 drug design. *Nature Rev Mol Cell Biol.* **23**, 21–39. https://doi.org/10.1038/s41580-021-00432-z.
52. Grellet, E., L'Hôte, I., Goulet, A., Imbert, I., (2022). Replication of the coronavirus genome: A paradox among positive-strand RNA viruses. *J. Biol. Chem.* **298**, https://doi.org/10.1016/j.jbc.2022.101923 101923.
53. Subissi, L., Posthuma, C.C., Collet, A., Zevenhoven-Dobbe, J.C., Gorbalenya, A.E., Decroly, E., Snijder, E.J., Canard, B., et al., (2014). One severe acute respiratory syndrome coronavirus protein complex integrates processive RNA polymerase and exonuclease activities. *PNAS* **111**, E3900–E3909.
54. Kirchdoerfer, R.N., Ward, A.B., (2019). Structure of the SARS-CoV nsp12 polymerase bound to nsp7 and nsp8 co-factors. *Nature Commun.* **10**, 2342. https://doi.org/10.1038/s41467-019-10280-3.
55. Peti, W., Johnson, M.A., Herrmann, T., Neuman, B.W., Buchmeier, M.J., Nelson, M., Joseph, J., Page, R., et al., (2005). Structural Genomics of the Severe Acute Respiratory Syndrome Coronavirus: Nuclear Magnetic Resonance Structure of the Protein nsP7. *J. Virol.* **79**, 12905–12913.
56. Deming, D.J., Graham, R.L., Denison, M.R., Baric, R.S., (2007). Processing of Open Reading Frame 1a Replicase Proteins nsp7 to nsp10 in Murine Hepatitis Virus Strain A59 Replication. *J Virol.* **81**, 10280–10291. https://doi.org/10.1128/JVI.00017-07.
57. Zhang, J., Yuan, S., Peng, Q., Ding, Z., Hao, W., Peng, G., Xiao, S., Fang, L., (2022). Porcine Epidemic Diarrhea Virus nsp7 Inhibits Interferon-Induced JAK-STAT Signaling through Sequestering the Interaction between KPNA1 and STAT1. *J Virol.*, e00400–e422. https://doi.org/10.1128/jvi.00400-22.
58. Cheng, R., Liu, J., Wang, L., Forstner, M.B., Rozovsky, S., (2021). Reengineering the Site-Specific Incorporation of Selenocysteine Into Proteins. *In: Encyclopedia of Biological Chemistry III*. Elsevier, pp. 757–765. https://doi.org/10.1016/B978-0-12-819460-7.00135-3.
59. Wessjohann, L.A., Schneider, A., Abbas, M., Brandt, W., (2007). Selenium in chemistry and biochemistry in comparison to sulfur. *Biol. Chem.* **388**, 997–1006. https://doi.org/10.1515/BC.2007.138.
60. Liu, J., Srinivasan, P., Pham, D.N., Rozovsky, S., (2012). Expression and purification of the membrane enzyme selenoprotein K. *Protein Expr. Purif.* **86**, 27–34. https://doi.org/10.1016/j.pep.2012.08.014.
61. Zhang, Z., Liu, J., Rozovsky, S., (2018). Preparation of selenocysteine-containing forms of human SELENOK and SELENOS. *Methods Mol. Biol.* **1661**, 241–263. https://doi.org/10.1007/978-1-4939-7258-6_18.
62. Cheng, R., Liu, J., Daithankar, V., Rozovsky, S., (2022). Applying selenocysteine-mediated expressed protein ligation to prepare the membrane enzyme selenoprotein S. *In: Methods in Enzymology*. Elsevier, pp. 159–185. https://doi.org/10.1016/bs.mie.2021.10.023.
63. Go, C.D., Knight, J.D.R., Rajasekharan, A., Rathod, B., Hesketh, G.G., Abe, K.T., Youn, J.-Y., Samavarchi-Tehrani, P., et al., (2021). A proximity-dependent biotinylation map of a human cell. *Nature* **595**, 120–124. https://doi.org/10.1038/s41586-021-03592-2.
64. Shchedrina, V.A., Zhang, Y., Labunskyy, V.M., Hatfield, D. L., Gladyshev, V.N., (2010). Structure-function relations, physiological roles, and evolution of mammalian ER-resident selenoproteins. *Antioxid. Redox Signal.* **12**, 839–849. https://doi.org/10.1089/ars.2009.2865.
65. Jumper, J., Evans, R., Pritzel, A., Green, T., Figurnov, M., Ronneberger, O., Tunyasuvunakool, K., Bates, R., et al., (2021). Highly accurate protein structure prediction with AlphaFold. *Nature*. https://doi.org/10.1038/s41586-021-03819-2.
66. Baek, M., DiMaio, F., Anishchenko, I., Dauparas, J., Ovchinnikov, S., Lee, G.R., Wang, J., Cong, Q., et al., (2021). Accurate prediction of protein structures and interactions using a three-track neural network. *Science* **7**
67. Humphreys, I.R., Pei, J., Baek, M., Krishnakumar, A., Anishchenko, I., Ovchinnikov, S., Zhang, J., Ness, T.J., et al., (2021). Computed structures of core eukaryotic

protein complexes. *Science* **374**, eabm4805. https://doi.org/10.1126/science.abm4805.
68. Christensen, L.C., Jensen, N.W., Vala, A., Kamarauskaite, J., Johansson, L., Winther, J.R., Hofmann, K., Teilum, K., et al., (2012). The human selenoprotein VCP-interacting membrane protein (VIMP) is non-globular and harbors a reductase function in an intrinsically disordered region. *J. Biol. Chem.* **287**, 26388–26399. https://doi.org/10.1074/jbc.M112.346775.
69. Madru, C., Tekpinar, A.D., Rosario, S., Czernecki, D., Brûlé, S., Sauguet, L., Delarue, M., (2021). Fast and efficient purification of SARS-CoV-2 RNA dependent RNA polymerase complex expressed in Escherichia coli. *PLoS One* **16** https://doi.org/10.1371/journal.pone.0250610.
70. Kao, A., Chiu, C., Vellucci, D., Yang, Y., Patel, V.R., Guan, S., Randall, A., Baldi, P., et al., (2011). Development of a Novel Cross-linking Strategy for Fast and Accurate Identification of Cross-linked Peptides of Protein Complexes M110.002170 *Mol. Cell. Proteom.* **10** https://doi.org/10.1074/mcp.M110.002212.
71. Müller, M.Q., Dreiocker, F., Ihling, C.H., Schäfer, M., Sinz, A., (2010). Cleavable Cross-Linker for Protein Structure Analysis: Reliable Identification of Cross-Linking Products by Tandem MS. *Anal. Chem.* **82**, 6958–6968. https://doi.org/10.1021/ac101241t.
72. Keller, A., Chavez, J.D., Felt, K.C., Bruce, J.E., (2019). Prediction of an Upper Limit for the Fraction of Interprotein Cross-Links in Large-Scale in Vivo Cross-Linking Studies. *J. Proteome Res.* **18**, 3077–3085. https://doi.org/10.1021/acs.jproteome.9b00189.
73. Shchedrina, V.A., Everley, R.A., Zhang, Y., Gygi, S.P., Hatfield, D.L., Gladyshev, V.N., (2011). Selenoprotein K binds multiprotein complexes and is involved in the regulation of endoplasmic reticulum homeostasis. *J. Biol. Chem.* **286**, 42937–42948. https://doi.org/10.1074/jbc.M111.310920.
74. Shi, F.-S., Yu, Y., Li, Y.-L., Cui, L., Zhao, Z., Wang, M., Wang, B., Zhang, R., et al., (2022). Expression Profile and Localization of SARS-CoV-2 Nonstructural Replicase Proteins in Infected Cells e00744-22 *Microbiol. Spectr.*. https://doi.org/10.1128/spectrum.00744-22.
75. Yang, Z., Zhang, X., Wang, F., Wang, P., Kuang, E., Li, X., (2020). Suppression of MDA5-mediated antiviral immune responses by NSP8 of SARS-CoV-2. *Microbiology*. https://doi.org/10.1101/2020.08.12.247767.
76. Wang, W., Zhou, Z., Xiao, X., Tian, Z., Dong, X., Wang, C., Li, L., Ren, L., et al., (2021). SARS-CoV-2 nsp12 attenuates type I interferon production by inhibiting IRF3 nuclear translocation. *Cell Mol Immunol.* **18**, 945–953. https://doi.org/10.1038/s41423-020-00619-y.
77. Wierbowski, S.D., Liang, S., Liu, Y., Chen, Y., Gupta, S., Andre, N.M., Lipkin, S.M., Whittaker, G.R., et al., (2021). A 3D structural SARS-CoV-2–human interactome to explore genetic and drug perturbations. *Nature Methods.* **18**, 1477–1488. https://doi.org/10.1038/s41592-021-01318-w.
78. Chen, J., Malone, B., Llewellyn, E., Grasso, M., Shelton, P. M.M., Olinares, P.D.B., Maruthi, K., Eng, E.T., et al., (2020). Structural Basis for Helicase-Polymerase Coupling in the SARS-CoV-2 Replication-Transcription Complex. *Cell* **182**, 1560–1573.e13. https://doi.org/10.1016/j.cell.2020.07.033.
79. Yan, L., Zhang, Y., Ge, J., Zheng, L., Gao, Y., Wang, T., Jia, Z., Wang, H., et al., (2020). Architecture of a SARS-CoV-2 mini replication and transcription complex. *Nature Commun.* **11**, 5874. https://doi.org/10.1038/s41467-020-19770-1.
80. Wang, Q., Wu, J., Wang, H., Gao, Y., Liu, Q., Mu, A., Ji, W., Yan, L., et al., (2020). Structural Basis for RNA Replication by the SARS-CoV-2 Polymerase. *Cell*. https://doi.org/10.1016/j.cell.2020.05.034.
81. Yin, W., Mao, C., Luan, X., Shen, D.D., Shen, Q., Su, H., Wang, X., Zhou, F., et al., (2020). Structural basis for inhibition of the RNA-dependent RNA polymerase from SARS-CoV-2 by remdesivir. *Science*. https://doi.org/10.1126/science.abc1560.
82. Peng, Q., Peng, R., Yuan, B., Zhao, J., Wang, M., Wang, X., Wang, Q., Sun, Y., et al., (2020). Structural and Biochemical Characterization of the nsp12-nsp7-nsp8 Core Polymerase Complex from SARS-CoV-2. *Cell Rep.* **31** https://doi.org/10.1016/j.celrep.2020.107774.
83. Jochheim, F.A., Tegunov, D., Hillen, H.S., Schmitzová, J., Kokic, G., Dienemann, C., Cramer, P., (2021). The structure of a dimeric form of SARS-CoV-2 polymerase. *Commun. Biol.* **4** https://doi.org/10.1038/s42003-021-02529-9.
84. Perry, J.K., Appleby, T.C., Bilello, J.P., Feng, J.Y., Schmitz, U., Campbell, E.A., (2021). An atomistic model of the coronavirus replication-transcription complex as a hexamer assembled around nsp15. *J. Biol. Chem.* **297**, https://doi.org/10.1016/j.jbc.2021.101218 101218.
85. Zeng, H., Gao, X., Xu, G., Zhang, S., Cheng, L., Xiao, T., Zu, W., Zhang, Z., (2022). SARS-CoV-2 helicase NSP13 hijacks the host protein EWSR1 to promote viral replication by enhancing RNA unwinding activity. *Infectious Med.* **1**, 7–16. https://doi.org/10.1016/j.imj.2021.12.004.
86. Lee, J.H., Kwon, J.H., Jeon, Y.H., Ko, K.Y., Lee, S.R., Kim, I.Y., (2014). Pro178 and Pro183 of selenoprotein S are essential residues for interaction with p97(VCP) during endoplasmic reticulum-associated degradation. *J. Biol. Chem.* **289**, 13758–13768. https://doi.org/10.1074/jbc.M113.534529.
87. Mendonça, L., Howe, A., Gilchrist, J.B., Sheng, Y., Sun, D., Knight, M.L., Zanetti-Domingues, L.C., Bateman, B., et al., (2021). Correlative multi-scale cryo-imaging unveils SARS-CoV-2 assembly and egress. *Nature Commun.* **12**, 4629. https://doi.org/10.1038/s41467-021-24887-y.
88. Lee, J.H., Jang, J.K., Ko, K.Y., Jin, Y., Ham, M., Kang, H., Kim, I.Y., (2019). Degradation of selenoprotein S and selenoprotein K through PPARγ-mediated ubiquitination is required for adipocyte differentiation. *Cell Death Differ.* **26**, 1007–1023. https://doi.org/10.1038/s41418-018-0180-x.
89. Kim, C.Y., Kim, K.H., (2013). Dexamethasone-induced selenoprotein S degradation is required for adipogenesis. *J. Lipid Res.* **54**, 2069–2082. https://doi.org/10.1194/jlr.M034603.
90. Schagger, H., (2006). Tricine-SDS-PAGE. *Nature Protoc.* **1**, 16–22. https://doi.org/10.1038/nprot.2006.4.
91. Jurrus, E., Engel, D., Star, K., Monson, K., Brandi, J., Felberg, L.E., Brookes, D.H., Wilson, L., et al., (2018). Improvements to the APBS biomolecular solvation software suite. *Protein Sci.* **27**, 112–128. https://doi.org/10.1002/pro.3280.
92. Humphrey, W., Dalke, A., Schulten, K., (1996). VMD: Visual molecular dynamics. *J. Mol. Graph.* **14**, 33–38. https://doi.org/10.1016/0263-7855(96)00018-5.